THE ASTROPHYSICAL JOURNAL, 411:266–273, 1993 July 1

2–12.5 MICRON IMAGING OF IRAS 21282+5050: THE STRUCTURE OF A YOUNG PLANETARY NEBULA

M. MEIXNER,[1,2] C. J. SKINNER,[2,3] P. TEMI,[4] D. RANK,[4] JESSE BREGMAN,[4] J. R. BALL,[3,5]
E. KETO,[2,6] J. F. ARENS,[7] AND J. G. JERNIGAN[7]
Received 1992 October 29; accepted 1993 January 5

ABSTRACT

We present 3.3, 8.5, 10.0, 11.3, and 12.5 μm narrow-band ($\Delta\lambda/\lambda \approx 3\%$–$10\%$) and K-band (2.2 μm) high spatial resolution images of IRAS 21282+5050 and a 6 cm flux density measurement. The new infrared images reveal a toroidal dust nebula, 4″.5 × 6″, P.A. 165°, with two prominent emission peaks aligned almost E-W and separated by 1″.7–2″.1; a remarkably similar structure to that observed in NGC 7027. From the 6 cm flux density and the dust nebula size, we derive an electron density of 3.6×10^3 cm^{-3} for the central ionized region. Comparison of these images with a published CO 1–0 map suggests that the structure of this dusty, ionization-bounded planetary nebula may reflect the density inhomogeneities of the progenitor's wind. Only slight spatial differences are discernible between the K-band and 10 μm "dust" continuum images and the 3.3, 11.3, and 12.5 μm unidentified infrared (UIR) emission-band images which have been attributed to polycyclic aromatic hydrocarbons (PAHs). This tight spatial correlation suggests that the K-band and 10 μm emission also arises from PAHs.

Subject headings: infrared: interstellar: continuum — planetary nebulae: individual (IRAS 21282+5050)

1. INTRODUCTION

IRAS 21282+5050 is a young, carbon-rich planetary nebula (PN) discovered by the *IRAS* satellite (Atlas of Low-Resolution *IRAS* Spectra 1986). The *IRAS* Low-Resolution Spectrometer (LRS) spectrum reveals strong features at 7.7, 8.6, 11.3 and 12 μm, attributed to polycyclic aromatic hydrocarbons (PAHs; Allamandola, Tielens, & Barker 1989; Leger & Puget 1984). In fact, this object has been the subject of several spectroscopic observations aimed at understanding the carriers of these mid-IR features and the corresponding near-IR features around 3.3 μm (de Muizon et al. 1986, 1990; Nagata et al. 1988; Roche, Aitken, & Smith 1991). We will refer to these features as the PAH bands throughout the rest of the paper.

Optical spectroscopy by Cohen & Jones (1987, hereafter CJ) first identified IRAS 21282 as a bright unresolved PN (less than 1″.2) with modest excitation surrounding an O7(f)-[WC11] central star. The PN nucleus suffers an A_V of 5.7 ± 0.1 mag. From the nebular emission lines a systemic $V_{\rm hel} = 8$ km s^{-1} is estimated; however, the central star has a systemic velocity of -12.3 km s^{-1}, which may indicate an interaction with a binary companion (CJ). The diffuse interstellar bands (DIBs) were observed toward this object by CJ who suggest that the DIBS are associated with the PAH emission of the nebula.

CO $J = 1$–0 and 2–1 observations by Likkel et al. (1988) marginally resolve a molecular circumstellar envelope ($\approx 10''$ FWHM) expanding at a velocity of 16 km s^{-1} with a $V_{\rm LSR} = 18$ km s^{-1} ($V_{\rm hel} = 4$ km s^{-1}). High resolution ($\sim 4''$) CO $J = 1$–0 interferometer maps by Shibata et al. (1989) show a clumpy expanding shell elongated N-S. The observed structure is interpreted by the authors to be an expanding torus with its polar axis aligned E-W and lying in the plane of the sky.

Most recently, K and L band imaging and spectroscopic observations of IRAS 21282 reveal a small ($\sim 5''$) dust nebula surrounding the central star with two peaks oriented almost east-west (Bregman et al. 1992). In addition, that study suggests that the 3.3 μm PAH emission extends up to $\sim 25''$ from the central star.

At the time of the observations presented in this paper, the structure of IRAS 21282 was thought to be an unresolved H II region (from CJ) surrounded by the remnant molecular envelope (Likkel et al. 1988). Hence, part of the motivation for imaging IRAS 21282 in the infrared was to determine the structure of the warm dust shell and how it related to the other components. Furthermore, imaging IRAS 21282 in the various PAH bands and nearby "continuum" wavelengths would compliment previous spectroscopic studies of these features. In particular, we wanted to determine if the size and shape of the nebula changed in the different PAH features and continuum bands, which one might expect if the features were excited by different wavelength photons or arose from different dust species. Such differences have been observed in other PN (e.g., Hora et al. 1990 and Woodward et al. 1989).

2. OBSERVATIONS AND RESULTS

2.1. *Mid-Infrared Images*

The 8.5, 10, 11.3, and 12.5 μm images of IRAS 21282 were taken at the NASA Infrared Telescope Facility (IRTF) on 1991 August 1, using the Berkeley Mid-IR array camera (Arens et al. 1987a, b; Keto et al. 1992). Image wavelength and bandwidth was determined by a circular variable filter with $\Delta\lambda/\lambda = 10\%$. The 10 μm camera contained a Hughes 10 × 64 pixel Si:Ga detector, and the pixel size was set at 0″.39. The mid-IR images were taken using standard chop and nod techniques at a chopper frequency of 6.5 Hz (cf. Ball et al. 1992). Total on-source integration time was 30 s at 8.5, 11.3, and 12.5 μm and 56 s at 10 μm resulting in an rms (1 σ) sky noise of ~ 10 mJy

[1] Department of Astronomy, University of California, Berkeley, CA 94720.
[2] Visiting Astronomer at the Infrared Telescope Facility.
[3] Institute of Geophysics & Planetary Physics and Laboratory for Experimental Astrophysics, L-413, LLNL P.O. Box 808, Livermore, CA 94550.
[4] Lick Observatory/UCO, University of California, Santa Cruz, CA 95060.
[5] 605 Lake Forest Drive, Vicksburg, MS 39180.
[6] L-59, LLNL P.O. Box 808, Livermore, CA 94550.
[7] Space Sciences Laboratory, University of California, Berkeley, CA 94720.

pixel^{-1} (or 65 mJy arcsec^{-2}). Images were flat-fielded by dividing by a normalized image of the sky, which provides a uniform illumination of the chip. We have tested this technique on images of a star moved up and down the long axis of the chip, and have found that it flattens the images so that the counts in each pixel are within $\sim$5% of the average counts. The M0 III star, β Peg (Cohen et al. 1993), was imaged as the flux calibrator and point spread function (psf, FWHM $\approx$0.″8) standard just after the IRAS 21282 observations and at a very close air mass to it, making correction for the air mass in flux calibration negligible. The mid-IR chip was oriented so that the long side of the chip is aligned NS. For each mid-IR image of IRAS 21282 and for the 10 and 12.5 μm image of β Peg, a three panel E-W mosaic has been made consisting of at least two independent observations at each position. We assembled the panels into final mosaiced images which are displayed in Figure 1. Total fluxes at each wavelength, in excellent agreement with previous observations (e.g., *IRAS* LRS spectrum), are listed in Table 1. In order to better discern the size and structure of the emission nebula, IRAS 21282 images were deconvolved at each wavelength using the Lucy-Richardson algorithm as realized in the IRAF package. The deconvolution algorithm was iterated approximately 30 times for all images. The results of the deconvolution are presented in Figure 2. IRAF[8] was employed for all data reduction.

2.2. *Near-Infrared Images*

The K-band (2.2 μm) and 3.3 μm narrow-band ($\Delta\lambda/\lambda = 3\%$) images were obtained at Lick Observatory with the Shane 3 telescope using the LIRC1 (Gilmore, Koo, & Rank 1991) and NASA/Lick infrared cameras, respectively, on 1991 July 29 and 1992 September 19. The K-band image we present here is the same observation that was presented by Bregman et al. (1992); however, we present it without the central star subtracted. The LIRC1 and NASA/Lick cameras used 128 × 128 HgCdTe and InSb arrays with pixel sizes of 0.″38 and 0.″32, respectively. The images were taken in a staring mode nodding the telescope at 5 to 10 s intervals to record frames on and off the nebula for sky subtraction. The 2.2 and 3.3 μm images used source-sky integration times of 10 s and 4.5 minutes, respectively. A CCD TV autoguider was used to maintain the position of IRAS 21282 within a small fraction of the 2.2 and 3.3 μm point source image diameter. White dwarf stars, EG 141 and V411 Tau (Zuckerman & Becklin 1987) and the A2 I star, α Cyg (Tokunaga 1988), were used to determine the psf (FWHM $\sim$ 1.″2) and primary flux calibration at 2.2 and 3.3 μm. These measurements were taken close in time and air mass to IRAS 21282 making correction for air mass negligible. Flat-field corrections accurate to a few percent for each near-IR camera were obtained from dome or sky frames recorded periodically during each night. Total fluxes are listed in Table 1. Final images, reduced with IRAF, are shown in Figure 1 and deconvolved images, using the same criteria and algorithm as for the mid-IR images (§ 2.1) are displayed in Figure 2. A poorer quality 3.45 μm image was obtained through thin clouds and is not shown, but was essentially identical to the 3.3 μm image.

[8] Image Reduction and Analysis Facility is distributed by the National Optical Astronomy Observatories, which is operated by the Association of Universities for Research in Astronomy, Inc., under contract to the National Science Foundation.

2.3. 6 cm *Flux Density*

We obtained a 6 cm flux density measurement of IRAS 21282 at Jodrell Bank employing a Broad-Band Interferometer (BBI; cf. Padin, Davis, & Lasenby 1987) consisting of the Mark I 76 m and Mk II 32 m telescopes. The bandwidth of the interferometer at 5 GHz is 384 MHz. A single short baseline of 424 m producing a resolution of 30″ at 5 GHz was employed and hence no spatial information was obtained. With an integration time of 60 minutes, we measured a flux of 8 $\pm$ 0.8 mJy (cf. Table 1). Flux calibration was achieved using VLA 6 cm standards.

3. DISCUSSION

3.1. *Distance to* IRAS 21282+5050

Distances to PN are notoriously uncertain except for some well studied cases. For example, NGC 7027 is measured to be 880 $\pm$ 100 pc (Masson 1989) from the proper motion of its expanding H II region. The distance to IRAS 21282 was estimated to be less than 2 kpc by Likkel et al. (1988) who argued that because the object has a positive systemic velocity in a direction where most objects had negative velocities (due to Galactic rotation), the object must be close to the sun. Shibata et al. (1989) also considered 2 kpc as a reasonable distance arguing that the dynamical age of the nebula and the age of the central star from the Schönberner (1983) tracks agree best for a distance close to 2 kpc. Since IRAS 21282 and NGC 7027 appear to be very similar, e.g., both are young carbon-rich PN, it is tempting to consider that the neutral gas shell as detected in CO is also very similar and that by comparing the two one can bootstrap the distance of IRAS 21282 from the well-known distance of NGC 7027. The neutral envelope of NGC 7027 has a CO 1–0 intensity of 280 K km s^{-1} (Huggins & Healy 1989) and a CO 1–0 size of $\sim$70″ (Bieging, Wilner, & Thronson

TABLE 1

OBSERVED QUANTITIES OF IRAS 21282+5050

Wavelength	F_ν(Jy)[a]	Magnitude	Major Axis[b]	Minor Axis[b]	Peak Separation[c]
2.2 μm	0.14 $\pm$ 0.03	9.15 $\pm$ 0.25	5.″3	4.″6	...
3.3 μm	1.4 $\pm$ 0.3	5.9 $\pm$ 0.3	5.8	4.8	1.″7 $\pm$ 0.″06
8.5 μm	37 $\pm$ 4	0.38 $\pm$ 0.1	6	4.4	1.7 $\pm$ 0.17
10 μm	20 $\pm$ 2	0.81 $\pm$ 0.1	5.5	4.6	1.7 $\pm$ 0.08
11.3 μm	42 $\pm$ 4	−0.26 $\pm$ 0.2	6	4.2	2.1 $\pm$ 0.08
12.5 μm	50 $\pm$ 5	−0.7 $\pm$ 0.1	6	4.2	1.9 $\pm$ 0.08
6 cm	8 $\pm$ 0.8 × 10^{-3}	...	...	...	...

[a] Quoted errors include a 10% error in photometry for the mid-IR and 20% for the near-IR.
[b] Sizes are measured at the lowest contour level in Fig. 2.
[c] Quoted errors are derived from variations encountered in measuring the peak separations in different exposures of that image.

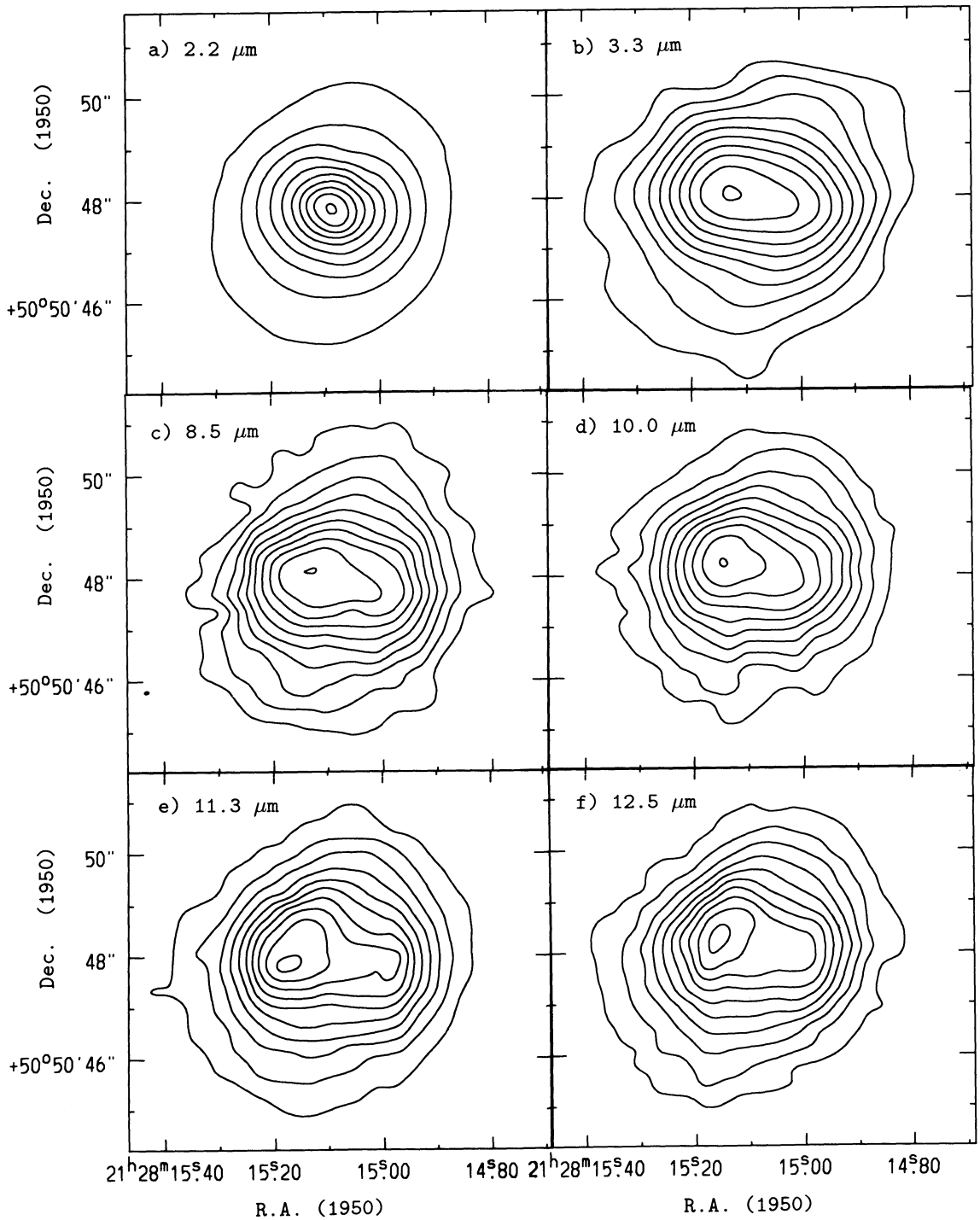

FIG. 1.—2.2–12.5 μm images of IRAS 21282+5050 (*a–f*) revealing an elliptical PAH emission nebula (4.″5 × 6″, P.A. 165°) showing two peaks aligned approximately E-W. The center of the 2.2 μm image is dominated by the star, which is overpowered by the PAH emission at the other wavelengths. The value of the contour levels in mJy arcsec^{-2} are given as: lowest contour, interval. (*a*) 2.2 μm: 1.93, 3.59; (*b*) 3.3 μm: 15.4, 14.5; (*c*) 8.5 μm: 266, 264; (*d*) 10 μm: 193, 199; (*e*) 11.3 μm: 372, 375; (*f*) 12.5 μm: 449, 449.

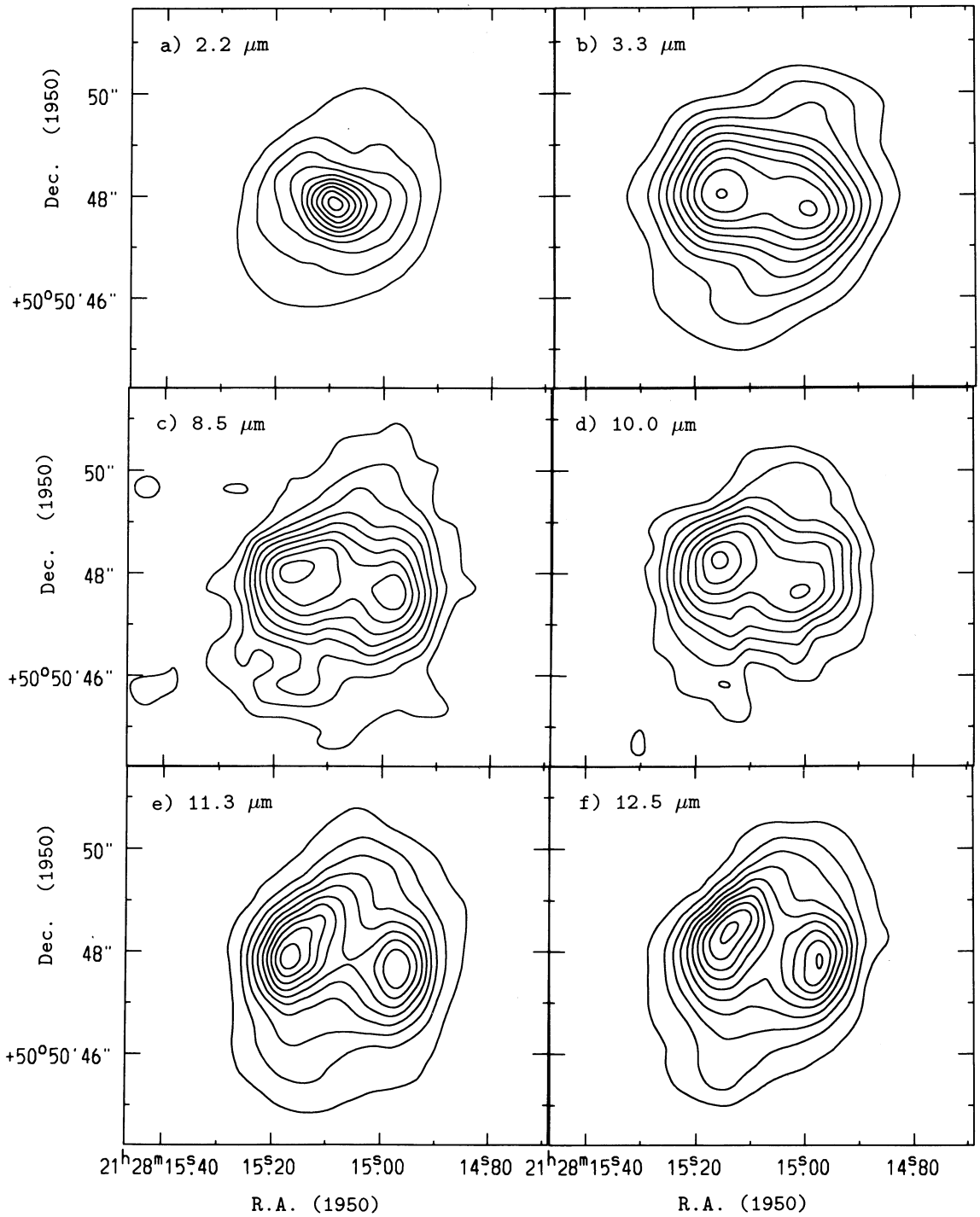

FIG. 2.—Deconvolved images of IRAS 21282+5050 (from Figs. 1*a*–1*f*) which clearly resolve the double-peaked structure of the planetary nebula in panels (*b*)–(*f*) and the star in panel (*a*). The value of the contour levels in mJy arcsec^{-2} are given as: lowest contour, interval. (*a*) 2.2 μm: 1.93, 8.05; (*b*) 3.3 μm: 30.2, 30.2; (*c*) 8.5 μm: 731, 452; (*d*) 10 μm: 664, 359; 11.3 μm: 744, 744; (*f*) 12.5 μm: 797, 870.

1991). IRAS 21282 has a CO 1–0 line intensity of 40 K km s^{-1} (Likkel et al. 1988) and a CO 1–0 size greater than 14″ (Shibata et al. 1989, a lower limit because the interferometer maps resolve some flux on larger scales). Since intensity scales as the distance squared, one would obtain a distance of ~2.3 kpc for IRAS 21282. This distance also results in a CO 1–0 envelope size of 26″ for IRAS 21282, which is reasonable. Although by no means conclusive, this comparison also suggests a value of ~2 kpc for the distance to the nebula which we adopt in this paper.

3.2. *Source Structure*

In all four of the observed PAH bands, 3.3, 8.5, 11.3, and 12.5 μm, and in the 10 μm continuum a very similar structure for IRAS 21282 appears: an elliptically shaped nebula with two prominent peaks lying almost east-west (Figs. 1 and 2). As measured in the deconvolved images (Fig. 2), the size of the dust nebula is 4.″5 by 6″, P.A. 165° (~1 by 2 × 10^{17} cm) and the peaks are separated by 1.″7 (~5 × 10^{16} cm) at 10 μm and 2.″1 (~6 × 10^{16} cm) at 11.3 μm.

In contrast, the K band continuum image of IRAS 21282 (Figs. 1*a*–2*a*) shows a strong central point source—the PN nucleus—in addition to the extended component—the dust nebula observed at the other wavelengths. We know the point source is the PN nucleus because the K-band magnitude of the unresolved core, 10.5, is what we would expect from the V-band magnitude and reddening of the central star as measured by CJ. Specifically, the central star has an apparent V-band magnitude of 14.4, an $A_V \sim 5.8$ mag, an $E(B-V) = 1.88$, and a reddening, R, of 3.10 which agrees with the "standard" interstellar reddening law (CJ). From standard interstellar reddening curves (e.g., Johnson 1965), we find that $E(V-K) = 5.08$. Since an O7 star has an intrinsic V_0-K_0 of −0.94 (Johnson 1966), we calculate an expected K-band magnitude of 10.3 from $V-(V_0-K_0)-E(V-K)$; which is indeed very close to the value we measured. We do not see the reddened star in our 3.3 μm or mid-IR images because at these wavelengths the flux of the O7 star (~9–10 mag) is overpowered by the surrounding PAH/dust emission (~ −0.7–5.9 mag).

The extended structure at K-band, as shown in the deconvolved image (Fig. 2*a*), has an elliptical shape of similar size to that observed at the other IR wavelengths (4.″6 × 5.″3, P.A. 165°). Furthermore, there is an E-W bar near the star that is revealed as two peaks when the PN nucleus' flux is subtracted from the image (cf. Bregman et al. 1992). These two peaks are the same peaks observed in the PAH features and at 10 μm, and in Figure 3*a* we demonstrate how the 3.3 μm peaks straddle the central star. The image structure for the six infrared wavelengths is summarized in Table 1.

The morphology of the infrared emission in IRAS 21282 and the planetary nebula NGC 7027 is very similar. Both objects show double peaks and an elliptical nebula in the IR-continuum and in the PAH emission bands. In NGC 7027, the shape of the IR emission has been interpreted as emission from a toroid with its polar axis aligned nearly N-S (Graham et al. 1993; Woodward et al. 1989; Arens et al. 1984). The IR images of IRAS 21282 also suggest a toroid with its polar axis aligned N-S. It has been suggested that such toroidal structures in PN can be produced when a spherically symmetric fast wind from the PN nucleus interacts with the slower progenitor wind which developed an equatorial density enhancement on the asymptotic giant branch (AGB; e.g., Balick 1987). The influence of a binary companion, especially a common envelope binary, on the AGB mass loss could create an equatorial density enhancement (e.g., Soker & Harpaz 1992). If these

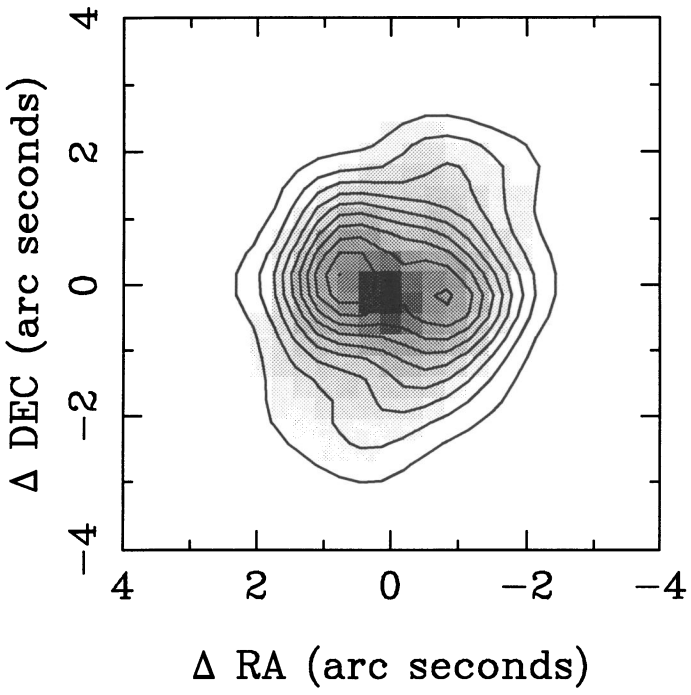

FIG. 3*a*

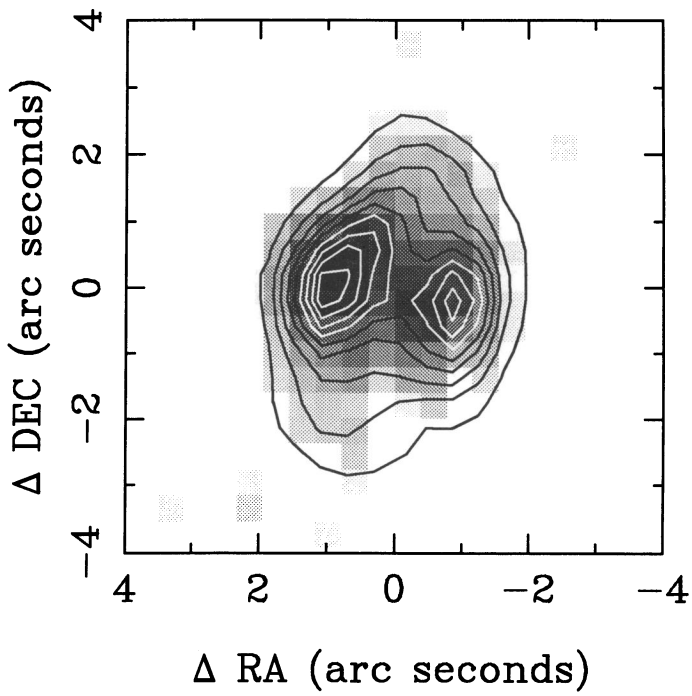

FIG. 3*b*

FIG. 3.—(*a*) 3.3 μm contours overlaid on the K-band image in gray scale. (*b*) 11.3 μm contours overlaid on the 10 μm image in gray scale; both the 11.3 and 10 μm images start at 20% of their respective peak values for an appropriate comparison.

models are correct, then IRAS 21282 should have a binary companion and it is interesting to note that CJ suggest that there may be a binary in IRAS 21282 because the stellar velocity is different than the nebula velocity by ~ 20 km s^{-1}.

A comparison of our IR images to the 6 and 2 cm VLA maps of Likkel et al. (1993) shows that the infrared and radio continuum emission have a very similar morphology, except the infrared emission is greater than 1″ larger in extent. Peaks appearing in the radio correspond to structure (peaks and extensions) seen in the infrared. Because the infrared images are so similar to the radio continuum, we can transfer the radio astrometry of the VLA maps to the mid-IR images and use these coordinates for a very exact comparison with the CO 1–0 interferometer maps of Shibata et al. (1989).

As shown in Figure 4, the 12.5 μm emission fills the central depression of the CO 1–0 channel map (Shibata et al. 1989) which is centered on the systemic velocity (16.9 km s^{-1}) and hence approximates a slice through the center of the molecular envelope. If the Shibata et al. (1989) interpretation of the CO maps is correct, then the molecular torus and infrared torus are perpendicular to each other which would be quite unusual for such a source. However, an alternative interpretation for the CO 1–0 map, that of an elliptical, clumpy envelope, can reconcile the geometries at 12.5 μm and CO. In fact, the two 12.5 μm peaks in IRAS 21282 are adjacent to the two northern CO peaks suggesting that these molecular clumps are associated with the east-west dust clumps we observe.

In NGC 7027, a similar interaction between the molecular circumstellar envelope and the central H II region and dust emission is observed. The molecular envelope in NGC 7027 surrounds the central H II region with a clumpy elliptical ring (Bieging et al. 1991; Graham et al. 1993), and there are dense CO clumps adjacent to the peaks observed in the radio continuum and infrared. These dense clumps are interpreted as equatorial density enhancements in the old AGB mass loss of NGC 7027 and as the ionization front progresses through the molecular envelope, the radio continuum and dust emission takes on the same shape as the molecular envelope.

By analogy, in IRAS 21282 the shape of the IR emission should reflect the structure of the old AGB wind expanding shell. Hence, from our mid-IR observations we would anticipate that the molecular torus in IRAS 21282 should be aligned N-S, not E-W as thought by Shibata et al. (1989). Perhaps the CO 1–0 interferometer map is misleading because it does not have sufficient UV coverage. Along these lines, we note that the interferometer map is missing $\sim 50\%$ of the total CO flux some of which could be distributed on small scales if the UV coverage is insufficient. Furthermore, we note that our images show a location for the central star ($\alpha = 21^h28^m15^s.1$, $\delta = 50°50'48''$, 1950) that is 1″ north of that assumed by Shibata et al. (1989) which is in slightly better agreement with the centroid of the CO emission. Nevertheless, the only conclusive way to determine the geometry of the molecular envelope is to make a CO 1–0 map of IRAS 21282 that contains all of the CO flux.

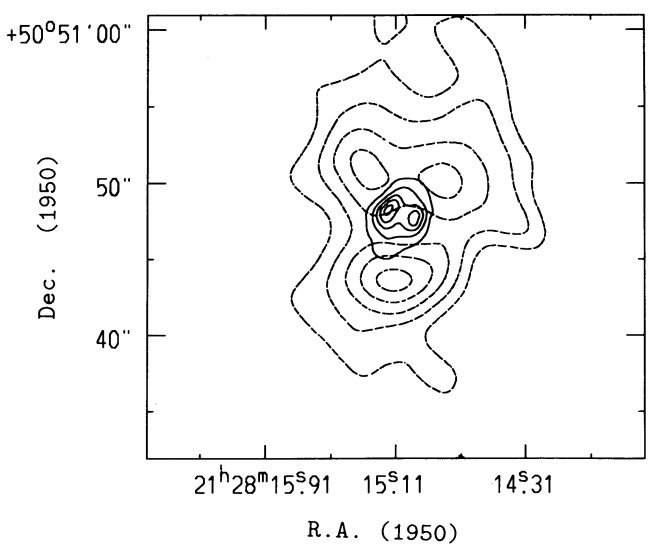

FIG. 4.—Deconvolved 12.5 μm image (*solid contours*) overlaid on the CO 1–0 16.9 km s^{-1} channel map (*dashed contours*) of Shibata et al. (1989).

3.3. *Electron Density*

An estimate of the electron density of the ionized gas in IRAS 21282 can be obtained from the 6 cm flux density, 8 mJy, and the nebula size as measured in the infrared images. First we calculate a free-free volume emissivity, ϵ_ν, of 3.39×10^{-33} ergs s^{-1} cm^{-3} Hz^{-1} sr^{-1} using the following equation: $\epsilon_\nu 4\pi V = 8$ mJy $4\pi D^2$. In this equation we assume D, distance to the nebula, is 2 kpc and V is $4\pi/3r^3$ ($r = 2''$, 0.0194 pc). Second, we use the standard formula for ϵ_ν (Allen 1965), and assuming an electron temperature of 10^4 K, we derive an electron density of 3.6×10^3 cm^{-3}. This value for the electron density is in agreement with Likkel et al. (1989) and reasonable for a young planetary nebula. However, because we do not account for clumping of the gas, the actual density could be higher than calculated.

3.4. *The Evolutionary State*

Shibata et al. (1989) claim that the dynamical age of IRAS 21282's CO envelope is 5×10^3 yr. They also suggested that it is younger than NGC 7027 because at the time the radio continuum emission was undetected. However, the dynamical age for NGC 7027 is also a few thousand years (Bieging et al. 1991) and we now know that IRAS 21282 has a detectable, although weak, radio continuum flux at 6 cm (this paper; Likkel et al. 1989, 1993). Hence, while IRAS 21282 may be less evolved than NGC 7027, it is not younger. The Schöberner (1983) tracks indicate that stars of larger progenitor mass evolve more quickly. Indeed, NGC 7027 has a luminosity of 6×10^3 $L_\odot$ and central star temperature of 2×10^5 K (Heap & Hintzen 1990; Jacoby 1988). IRAS 21282 has a luminosity of 2×10^3 $L_\odot$ at 2 kpc (cf. CJ) and an estimated central star temperature of 3×10^4 K. Furthermore, the pre-planetary mass-loss rate of NGC 7027, $\sim 2 \times 10^{-4}$ $M_\odot$ yr^{-1} (Jaminet et al. 1991), is larger than that of IRAS 21282, $\sim 6 \times 10^{-5}$ $M_\odot$ yr^{-1} (Likkel et al. 1988). All three quantities suggest that NGC 7027 had a more massive progenitor star resulting in a faster rate of evolution than IRAS 21282.

3.5. *The Nature of the Dust*

As noted in the introduction, IRAS 21282 has been a spectroscopic case study for understanding the carriers of the UIR emission features which have been attributed to PAHs. PAHs consist of small (~ 50 C atoms) aromatic carbon rings with hydrogen atoms attached to the outermost carbon atoms. Under the PAH hypothesis, the 3.3 μm feature is attributed to C-H stretching; the 8.5 μm feature to the C-H bending mode which occurs in the plane of the carbon ring; the 11.3 μm feature to the C-H bending mode which occurs out of the plane

of the carbon ring. Finally, the flux at 12.5 μm is attributed to a blend of C-H out of plane bending modes which form a plateau from 10 to 13 μm.

The 2.2 (K-band) and 10 μm bands are presumably free of emission from aromatic modes and have often been considered to be pure continuum. However, it is not known for certain that PAHs do not contribute to the emission in the K-band and 10 μm images. Certainly large PAH clusters could produce "dust" like continuum emission (Allamandola et al. 1989).

The strong correlation observed between K band and 3.3 μm and 10 and 11.3 μm images (Figs. 3*a* and 3*b*) may indicate that the PAHs play a role in the emission of infrared continuum radiation. At the very least the similarity in structure demonstrates that the emission is optically thin in the continuum and PAH emission bands. Although the size of the nebula, as judged by the lowest contour, appears to change with wavelength (cf. Table 1), these differences are not meaningful because the S/N of the images varies with wavelength, and effects the radial position of the lowest contour.

The K-band (2.2 μm) emission may arise from other sources. The K-band spectrum has been found to be featureless (M. Hoare, private communication), and hence the K-band image cannot be dominated by emission lines. It could be produced by a combination of free-free emission, emission from dust, or scattered light from the central star. If we assume that the K-band emission and 10 μm continuum arises from thermal emission from dust grains, then the dust would need to be extremely hot and at a uniform temperature throughout the nebula ($\sim$1000 K). Scattering by optically thin grain material could explain the K-band emission since we note that the emission from the nebula amounts to a bit less than half of the flux from the central star at K band. However, if the dust grains causing the scattering were a separate component from the PAHs, then the large ultraviolet (UV) dust opacity implied by a significant K-band scattering optical depth would leave little UV radiation to excite the PAH bands or ionize the gas. Therefore we consider it likely that the source of the K-band and 10 μm continuum lies within the gas containing the PAHs, and that the same material may be responsible for both the PAH bands and the infrared continuum emission.

Comparison of the five infrared images with each other reveals slight differences in the spatial distributions. The separation of the two prominent peaks is larger by 0".2–0".4, or one pixel, for the 12.5 and 11.3 μm images than for the 10 μm image (Table 1). In addition, the intensities of the peaks at 3.3, 11.3, and 12.5 μm are almost equal whereas in the 10 μm image the eastern peak is somewhat more dominant. Hence, while the emission at all four wavelengths may arise from the same carrier, there may be differences between the excitation of the bands and the "continuum."

Comparison of the PAH emission with the 6 cm radio continuum (Likkel et al. 1993) indicates that the PAH emission extends beyond the gas by 1" in diameter. The separation of the E-W peaks in the radio is $\sim$1".7 or roughly equal to the 10 μm image and slightly smaller than the separation of the 11.3 and 12.5 μm emission. Hence it seems that at least some of the PAH emission arises outside of the H II region. Studies of NGC 7027, particularly in the near-IR (Woodward et al. 1989; Graham et al. 1993), show that at least half of the PAH emission arises just outside the ionized gas. In the Orion Bar, where the physical scale is even better resolved, the PAH emission is clearly separated and just outside the ionized gas, and is interpreted as arising in the neutral zone (Sellgren, Tokunaga, & Nakada 1990). Thus while the PAH and radio continuum emissions appear very similar, they might, in fact, be separated at higher spatial resolutions.

4. CONCLUSIONS

1. We find that the structure of IRAS 21282 is remarkably similar across the infrared spectrum. The 3.3, 8.5, 10, 11.3, and 12.5 μm narrow-band ($\Delta\lambda/\lambda < 10\%$) images of the object reveal a 4".5 × 6", P.A. 165° nebula with two prominent peaks aligned almost E-W and separated by 1".7–2".1. The star as seen at K band is situated between the peaks. These images suggest a toroidal structure for IRAS 21282 which is similar to that observed in NGC 7027.

2. Comparison of the mid-IR images and CO 1–0 map reveals that the structure seen at the mid-IR wavelengths reflects the density inhomogeneities of the progenitor's mass loss. However, the toroidal structure seen in the mid-IR is perpendicular to that interpreted from the CO interferometer maps by Shibata et al. (1989). We suggest a different interpretation of the CO 1–0 maps, that of a clumpy elliptical envelope which seems to be more consistent with the geometry we observe in the infrared.

3. The infrared emission has a similar morphology but is slightly more extended ($\sim$1") than the radio continuum emission suggesting that at least some of the PAH emission arises outside of the ionized gas.

4. The strong correlation observed between 2.2–3.3 μm and 10–11.3 μm images indicates that PAHs may play a role in the emission of infrared continuum (2.2 and 10 μm) radiation. Slight spatial differences are discernible between the 10 μm continuum and the 3.3, 11.3, and 12.5 μm UIR bands attributed to PAHs. These differences may be due to differences in the excitation of the emission at the different wavelengths.

We would like to thank Lauren Likkel for permitting us to use her radio continuum images before their publication, Melvin Hoare for the useful information on the K-band spectrum and Kazunair Shibata for sending his CO data to us in digital form. Discussions with Lynne Deutsch, Joseph Hora, Bruce Hrivnak, and James Graham were very helpful. The observations could not have been obtained without the assistance of the IRTF, and Lick Observatory staffs. The Berkeley Mid-IR array camera is supported by the Institute of Geophysics and Planetary Physics and the Laboratory for Experimental Astrophysics of Lawrence Livermore National Laboratories. Work at LLNL was performed under the auspices of the US Department of Energy under contract no. W-7405-ENG-48.

REFERENCES

Allamandola, L. J., Tielens, A. G. G. M., & Barker, J. R. 1989, ApJS, 71, 733
Allen, C. W. 1965, Astrophysical Quantities (London: Athlone)
Arens, J. F., Jernigan, J. G., Ball, R., Peck, M. C., Gaalema, S., & Lacy, J. 1987a, in Infrared Astronomy with Arrays, ed. C. G. Wynn-Williams & E. Becklin (Honolulu: Univ. Hawaii), 256
Arens, J. F., Jernigan, J. G., Peck, M. C., Dobson, C. A., Kilk, E., Lacy, J., & Gaalema, S. 1987b, Appl. Optics, 26, 3846
Arens, J. F., Lamb, G. M., Peck, M. C., Moseley, H., Hoffman, W. F., Tresch-Feinberg, R. M., & Fazio, G. G. 1984, ApJ, 279, 685
Atlas of Low-Resolution *IRAS* Spectra. 1986, *IRAS* Science Team, prepared by F. M. Olnon & E. Raimond, A&AS, 65, 607
Balick, B. 1987, AJ, 94, 67
Ball, J. R., Arens, J. F., Jernigan, J. G., Keto, E., & Meixner, M. 1992, ApJ, 389, 616

Bieging, J. H., Wilner, D., & Thronson, H. A. 1991, ApJ, 379, 271
Bregman, J. D., Booth, J., Gilmore, D. K., Kay, L., & Rank, D. 1992, ApJ, 396, 120
Cohen, M., & Jones, B. F. 1987, ApJ, 321, L151 (CJ)
Cohen, M., Walker, R. G., Barlow, M. J., Deacon, J. R., Witteborn, F. C., Carbon, D. F., & Augason, G. C. 1993, in IAU Colloq. 136, Stellar Photometry—Current Techniques and Future Development, ed. I. Elliott, in press
de Muizon, M. J., d'Hendecourt, L. B., & Geballe, T. R. 1990, A&A, 227, 526
de Muizon, M., Geballe, T. R., d'Hendecourt, L. B., & Baas, F. 1986, ApJ, 306, L105
Gilmore, K., Koo, D., & Rank, D. 1991, in Proc. 10th Symp. on Photoelectronic Imaging Devices, ed. B. L. Morgan (Bristol: Inst. Phys.), 113
Graham, J., Serabyn, E., Herbst, T. M., Matthews, K., Neugebauer, G., Soifer, B. T., Wilson, T. D., & Beckwith, S. 1993, AJ, in press
Heap, S. R., & Hintzen, P. 1990, ApJ, 353, 200
Hora, J. L., Deutsch, L. K., Hoffman, W. F., & Fazio, G. G. 1990, ApJ, 353, 549
Huggins, P. J., & Healy, A. P. 1989, ApJ, 346, 201
Jacoby, G. H. 1988, ApJ, 333, 193
Jaminet, P. A., Danchi, W. C., Sutton, E. C., Russel, A. D. G., & Sandell, G. 1991, ApJ, 380, 461
Johnson, H. C. 1965, ApJ, 141, 923
Johnson, H. L. 1966, ARA&A, 4, 193
Keto, E., Ball, J. R., Arens, J. F., Jernigan, J. G., & Meixner, M. 1992, Int. J. Infrared Millimeter Waves, 13, 1709
Leger, A., & Puget, J. L. 1984, A&A, 137, L5
Likkel, L., Forveille, T., Omont, A., & Morris, M. 1988, A&A, 198, L1
Likkel, L., Morris, M., Omont, A., & Forveille, T. 1989, in IAU Colloq. 106, Evolution of Peculiar Red Giant Stars, ed. H. R. Johnson & B. Zuckerman (Cambridge: Cambridge Univ. Press), 233
Likkel, L., Morris, M., Kastner, J., Omont, A., & Forveille, T. 1993, in preparation
Masson, C. R. 1989, ApJ, 336, 294
Nagata, T., Tokunaga, T., Sellgren, K., Smith, R. G., Onaka, T., Nakada, Y., & Sakata, A. 1988, ApJ, 326, 157
Padin, S., Davis, R. J., & Lasenby, A. N. 1987, MNRAS, 224, 685
Roche, P. F., Aitken, D. K., & Smith, C. H. 1991, MNRAS, 252, 282
Schöberner, D. 1983, ApJ, 272, 708
Sellgren, K., Tokunaga, A. T., & Nakada, Y. 1990, ApJ, 349, 120
Shibata, K. M., Tamura, S., Deguchi, S., Hirano, N., Kameya, O., & Kasuga, T. 1989, ApJ, 345, L55
Soker, N., & Harpaz, A. 1992, PASP, 104, 923
Tokunaga, A. T. 1988, The Infrared Telescope Facility Photometry Manual (Washington DC: GPO)
Woodward, C. E., Pipher, J. L., Shure, M., Forrest, W. J., & Sellgren, K. 1989, ApJ, 342, 860
Zuckerman, B., & Becklin, E. E. 1987, ApJ, 319, L99